REPORT DOCUMENTATION PAGE

1a. REPORT SECURITY CLASSIFICATION	1b. RESTRICTIVE MARKINGS
UNCLASSIFIED	N/A

2a. SECURITY CLASSIFICATION AUTHORITY	3. DISTRIBUTION/AVAILABILITY OF REPORT
N/A	Approved for public release;
2b. DECLASSIFICATION/DOWNGRADING SCHEDULE	distribution unlimited.
N/A	

4. PERFORMING ORGANIZATION REPORT NUMBER(S)	5. MONITORING ORGANIZATION REPORT NUMBER(S)
NRL Memorandum Report 6067	

6a. NAME OF PERFORMING ORGANIZATION	6b. OFFICE SYMBOL (If applicable)	7a. NAME OF MONITORING ORGANIZATION
NAVAL RESEARCH LABORATORY Underwater Sound Reference Det	Code 5993	

6c. ADDRESS (City, State, and ZIP Code)	7b. ADDRESS (City, State, and ZIP Code)
P.O. Box 568337 Orlando, FL 32856-8337	

8a. NAME OF FUNDING/SPONSORING ORGANIZATION	8b. OFFICE SYMBOL (If applicable)	9. PROCUREMENT INSTRUMENT IDENTIFICATION NUMBER
OFFICE OF NAVAL RESEARCH	Code 01123	

8c. ADDRESS (City, State, and ZIP Code)	10. SOURCE OF FUNDING NUMBERS			
	PROGRAM ELEMENT NO.	PROJECT NO.	TASK NO.	WORK UNIT ACCESSION NO.
Arlington, VA 22217-5000	61153N		RR011-08-42	DN280-003 59-1472-0-0

11. TITLE (Include Security Classification)

DAMPING ANALYSIS OF WAVES IN FLUID-LOADED SINGLE AND CONSTRAINED PLATES

12. PERSONAL AUTHOR(S)
Pieter S. Dubbelday

13a. TYPE OF REPORT	13b. TIME COVERED	14. DATE OF REPORT (Year, Month, Day)	15. PAGE COUNT
Interim	FROM 10-86 TO 07-87	September 1, 1987	30

16. SUPPLEMENTARY NOTATION

17.	COSATI CODES		18. SUBJECT TERMS (Continue on reverse if necessary and identify by block number)
FIELD	GROUP	SUB-GROUP	Constrained layer damping Damping efficiency
20	01		Fluid loading of infinite plate
			Viscoelastic damping

19. ABSTRACT (Continue on reverse if necessary and identify by block number)

A hybrid model was developed for the analysis of constrained-layer damping whereby the base plate is described by exact elasticity theory, while the elastomer and constraining layers are analogous to Kerwin's model [J. Acoust. Soc. Am. **31**, 952-962 (1959)]. Under fluid loading, the success of the technique is measured by a damping efficiency, the ratio of loss in the elastomer to the total loss due to viscoelastic and radiation damping. This efficiency is usually evaluated by combining the viscoelastic loss from a composite plate in vacuum, for antisymmetric and symmetric waves separately with the radiation loss from a single fluid-loaded plate. This ignores the interaction of fluid and constrained plate. This study shows that at high and low frequencies discrepancies occur. Inclusion in the hybrid model of both flexural and extensional waves shows that at higher frequencies the presence of the two types of waves redistributes the energy across the plate. Thus it proves necessary to compute damping efficiency from analysis of the fluid-loaded composite plate with inclusion of both antisymmetric and symmetric waves. The report gives a

(continued on reverse)

20. DISTRIBUTION/AVAILABILITY OF ABSTRACT	21. ABSTRACT SECURITY CLASSIFICATION
[X] UNCLASSIFIED/UNLIMITED ☐ SAME AS RPT. ☐ DTIC USERS	UNCLASSIFIED

22a. NAME OF RESPONSIBLE INDIVIDUAL	22b. TELEPHONE (Include Area Code)	22c. OFFICE SYMBOL
Dr. Pieter S. Dubbelday	(305) 857-5197	NRL-USRD (Code 5993)

DD FORM 1473, 84 MAR

83 APR edition may be used until exhausted.
All other editions are obsolete.

SECURITY CLASSIFICATION OF THIS PAGE

UNCLASSIFIED

BLOCK 19 (continued):

tutorial review of the theory of wave propagation of straight-crested waves in a thin plate under fluid loading, before the hybrid theory for a fluid-loaded constrained plate is formulated.

Naval Research Laboratory

DAMPING ANALYSIS OF
FLEXURAL WAVES IN FLUID-LOADED
SINGLE AND CONSTRAINED PLATES

Pieter S. Dubbelday

Underwater Sound Reference Detachment
Naval Research Laboratory
P.O. Box 568337
Orlando, Florida 32856-8337

CONTENTS

BLANK PAGE

DAMPING ANALYSIS OF WAVES IN FLUID-LOADED
SINGLE AND CONSTRAINED PLATES

1. INTRODUCTION

The technique of constrained-layer damping is based on the addition of two layers to a base plate or bar: the first layer consists of a viscoelastic material with high loss factor in its shear modulus; the second layer is made of a stiff material that increases the shear in the viscoelastic layer, and thus promotes viscoelastic dissipation (Fig. 1).

An early analysis of constrained-layer damping was developed by E. M. Kerwin in 1959.[1] (A review of this technique is found in Ref. 2.) It is limited to thin-plate theory and does not include extensional waves. Recently, a model was developed by this author[3] that combines a description of the base plate by exact elasticity theory with the Kerwin treatment of the damping mechanism. The hybrid model lends itself quite readily to inclusion of the effect of fluid loading. It is often tacitly assumed that the radiation and viscoelastic damping in a fluid-loaded constrained plate are the same as, respectively, the radiation by a single plate in the fluid and the viscoelastic damping of a composite plate in vacuum. This ignores the interaction of fluid and composite plate, with possible consequences for the computation of attenuation and damping efficiency.

The present study develops a model for a hybrid constrained layer that is coupled to a fluid loading the plate on either or both faces. The model is formulated and applied to the attenuation of flexural waves in two cases: on one hand, the combination of the results for a fluid-loaded single plate with those for a composite plate in vacuum; on the other hand, the results for a fluid-loaded composite plate.

While studying the attenuation of wave propagation in a constrained layer under fluid loading, it was found that at low frequency (well below the coincidence frequency) the attenuation coefficient again reaches high values. There does not appear to be a wide-spread awareness of this phenomenon (which is also present for a single plate in a fluid), although it is found in the literature. Therefore, discussion of the fluid-loaded hybrid model is preceded by a discussion of the radiation by a single plate into a fluid according to thin-plate and exact-elasticity theories. This may also function as an introduction to the literature on the study of fluid-loaded thin plates.

2. FLEXURAL WAVES IN A FLUID-LOADED INFINITE THIN PLATE

2.1 Theory

The theory of the effect of fluid loading on the propagation of flexural waves in an infinite plate in the thin-plate approximation is extensively described in the literature. A general discussion of the problem may be found in Refs. 4 and 5. More detailed studies of the transfer function describing the forcing of fluid-loaded plates are given in Refs. 6 through 11.

For a discussion of the basic theory, the approach presented in Ref. 5 is followed here. A straight-crested flexural wave is traveling in the x-direction in an infinite plate with thickness h, density ρ_s, Young's modulus E, Poisson's ratio ν, and bending stiffness D; $D = Eh^3/12(1 - \nu^2)$. A fluid with wave speed c_o and density ρ_o is adjacent to the plate at the side of positive z; z is the coordinate perpendicular to the face of the plate; the surface of the plate exposed to the fluid is at z = h/2. The equation for the displacement w of the plate in the z direction is [5]

$$DV^4 w + \rho_s h \frac{\partial^2 w}{\partial t^2} = -p(z = h/2), \qquad (1)$$

where p is the pressure fluctuation in the fluid.

It may be noted here that the assumption of one-sided fluid loading is incompatible with the exclusion of extensional waves, but the ensuing discrepancy is small for the frequency range in which the thin-plate approximation is acceptable.

Continuity of normal displacement at the plate surface for z = h/2 leads to the boundary condition

$$\frac{\partial^2 w}{\partial t^2} = - 1/\rho_o \frac{\partial p}{\partial z} \text{ at } z = h/2. \qquad (2)$$

If the wave in the plate is harmonic, with time and x dependence expressed by $\exp i(\omega t - kx)$ (where k is the wavenumber), the corresponding compressional wave in the fluid is given by

$$p_+ = p_{o+} \exp i[\omega t - K_x x - K_z(z - h/2)], \qquad (3)$$

where the subscript + refers to the positive side of the plate, in anticipation of a later introduction of fluid at the negative side, indicated with subscript -. Here K_x and K_z are the components of the wave vector $\vec{K}$ in the fluid.

Matching the normal displacement at the boundary in plate and fluid leads to the condition that $k = K_x$. For reflection and transmission problems of plane waves k and $\vec{K}$ are real, and one may set $K_x = k_o \sin\theta$ and $K_z = k_o \cos\theta$, where k_o is the wavenumber in the fluid, with $k_o = \omega/c_o$, and θ the angle of incidence of the incoming wave. For a (decaying) free wave in a plate k, $\vec{K}$, and θ are complex.

2

To obtain a dispersion relation with real coefficients, one introduces a quantity τ related to K_z by $\tau = iK_z/k_o$ [5,10]. The boundary condition Eq. (2) then gives

$$\rho_o \omega^2 w = -k_o \tau p_+ \text{ at } z = h/2. \tag{4}$$

This enables one to replace p_+ in the wave equation [Eq. (1)] resulting in the dispersion relation

$$k^4 D - \rho_s h \omega^2 = \rho_o \omega^2 / (k_o \tau). \tag{5}$$

Since the wave in the fluid satisfies the Helmholtz equation, it follows that

$$K_x^2 + K_z^2 = k^2 - k_o^2 \tau^2 = k_o^2 \; ; \tag{6}$$

and thus one may substitute for k^2 in Eq. (5). This results in an equation for τ in the form

$$\tau^5 + 2\tau^3 + (1-\Omega^{-2})\tau - \epsilon\Omega^{-3} = 0 \; , \tag{7}$$

where Ω is a non-dimensional frequency $\Omega = \omega/\omega_c$. The angular frequency ω_c is that frequency for which the wave speed c_b of flexural waves in an unloaded thin plate is equal to the sound speed in the fluid (coincidence). Since

$$c_b^4 = \omega^2 D/(\rho_s h) \; , \tag{8}$$

one has

$$\omega_c^2 = \rho_s h c_o^4 / D \; . \tag{9}$$

The material parameter ϵ is given by

$$\epsilon = \rho_o c_o / (\omega_c \rho_s h) \; . \tag{10}$$

It is a measure for the influence of fluid loading; for $\epsilon = 0$, the wave speed c in the plate reduces to c_b, the wave speed in vacuum.

Alternatively ϵ may be written as

$$\epsilon = \frac{1}{\sqrt{12}} \, (\rho_o/\rho_s)(c_p/c_o) \, , \qquad (11)$$

and thus ϵ is independent of the plate thickness (as long as the plate may be considered "thin"; i.e., $kh/2 \ll 1$). Here c_p is the wave speed for extensional waves in a thin plate, $c_p^2 = E/[(1-\nu^2)\rho_s]$.

2.2 Character of the Roots of the Dispersion Relation

The dispersion relation [Eq. (7)] has five roots, not all of which have physical significance. Since its coefficients are real and the degree is odd, there is at least one real root. The quantity τ appears in the spatial dependence of the pressure in the fluid through the factor $\exp(-k_o \tau z)$ and thus only real roots with positive value for τ are physically acceptable, representing an evanescent wave in the positive z direction. If there are complex roots, they have to appear in pairs of complex conjugates; and the choice between the two members of a pair is dictated by the fact that one expects wave propagation in the positive z half-space when there is fluid only at that side of the plate. As a consequence, the imaginary part of τ should be positive. The constraint for the real part of τ issues from the following observation. If one considers a wave in the plate in the positive x direction, the complex wavenumber $k = k' - i\alpha$ is such that k' and α are both positive to assure a decrease of the wave amplitude in the x direction. Since $k^2 - k_o^2 \tau^2 = k_o^2$, the product of the real and imaginary parts of $k_o \tau$ is equal to $-\alpha k'$; thus, the real part of τ has to be negative. This in turn makes the imaginary part of K_z positive, and the amplitude of the wave increases with distance from the plate. This may appear physically unrealistic but it is not: Fig. 2 illustrates the explanation. Waves farther away from the plate originate in a location at the surface of the plate where the amplitude of the wave had a larger value.

The real root for τ represents a purely evanescent wave even for an infinite plate. The complex root poses a problem in interpretation: it has the appearance of a radiating root, but only for an infinite plate can this name be maintained. For an infinite plate, the distinction between nearfield and farfield is lost, and the "radiating" wave is always under the influence of the plate. For a finite plate, a wave with wave speed less than the plane wave speed c_o cannot exist in the farfield and thus is not truly a radiating wave. This was pointed out by Pierucci and Graham [12]. In the remainder of this report the term "radiation" will be used in connection with the presence of a valid complex root, but it should be realized that its behavior for a finite plate needs further scrutiny.

Setting $K_z = K_z' + iK_z''$ one may conclude that the angle δ of the "radiated waves" in the fluid with the normal is given by

$$\tan \delta = k'/K_z' \, , \qquad (12)$$

and the wave speed c_f of this wave in the fluid is

$$c_f = k_o c_o / [(k')^2 + (K_z')^2]^{1/2} .$$

(13)

Of course, these statements are all a consequence of the infinite-plate assumption.

This discussion may be illustrated by the asymptotic behavior of τ (= iK_z) for $\Omega \to 0$. On physical grounds one would expect that for low frequency the inertia of the plate may be ignored by dropping the second term of Eq. (1). If, moreover, the compressibility of the fluid is ignored, which is equivalent to setting $c/c_o \ll 1$, it follows that $\tau^2 + 1 \doteq \tau^2$, and the polynomial equation for τ reduces to $\tau^5 = \epsilon \Omega^{-3}$ [5]. The roots of this equation are

$$\tau = \epsilon^{1/5} \Omega^{-3/5} e^{2n\pi i/5} , \quad n = 0, 1, 2, 3, 4.$$

(14)

It follows from the above discussion that only the real root $\tau_1 = \epsilon^{1/5} \Omega^{-3/5}$ and the complex root $\tau_3 = \epsilon^{1/5} \Omega^{-3/5} (\cos 144^\circ + i \sin 144^\circ)$ are acceptable. One also infers that the non-dimensional attenuation for the radiating wave, given by α/k', approaches $\tan 36^\circ = 0.7265$ for $\Omega \to 0$.

One could also express the dispersion relation in terms of the wavenumber k in the plate. Since $k_o^2 \tau^2 = -K_z^2 = k^2 - k_o^2$, one can substitute for τ in Eq. (5) and square both sides of the equation to obtain a polynomial equation in terms of $\eta = (k/k_o)^2$.

$$\eta^5 - \eta^4 - 2\eta^3 \Omega^{-2} + 2\eta^2 \Omega^{-2} + \eta \Omega^{-4} - (\epsilon^2 + \Omega^2)\Omega^{-6} = 0$$

(15)

One finds five roots, of which only two are physically realistic: one real and one complex. Alternatively, one may solve Eq. (7) for τ and find η according to $\eta = \tau^2 + 1$. The proper k/k_o is obtained from η by realizing that k should have a positive real part to represent a wave propagating in the postive x direction. Thus from the five roots for η, one finds again five roots for k/k_o, two of which have physical meaning.

2.3 Computational Considerations

One may use a complex (polynomial) rootfinder for the roots $\tau = iK_z$ of Eq. (7) or $\eta = (k/k_o)^2$ of Eq. (15), and select the physically acceptable ones by the criteria developed above. Alternatively, one may avoid the introduction of spurious roots that squaring caused by choosing the proper branches in the substitution of τ according to $\tau = \pm \sqrt{(k/k_o)^2 - 1}$, again in

accordance with the selection rules developed before. The resulting equations are suitable to derive good first approximations and iterative schemes of computation.

If one defines the symbol $\sqrt{}$ to indicate the positive real root when the argument is real and positive, and the root with the positive real part when the argument is complex (conform to the sign convention in the Fortran square root routine), one obtains from Eq. (5) two equations for $(k/k_o)^2$: the first for complex k

$$i \sqrt{1-(k/k_o)^2} \left[1 - \Omega^2 (k/k_o)^4\right] + \epsilon/\Omega = 0 , \qquad (16)$$

and the second for real k

$$\sqrt{(k/k_o)^2 - 1} \left[1 - \Omega^2 (k/k_o)^4\right] + \epsilon/\Omega = 0 . \qquad (17)$$

One necessarily has $k > k_o$ for real k, since otherwise the first term of Eq. (17) would be imaginary and the second term real, which is impossible.

The real root for $k/k_o = c_o/c$ may be computed from Eq. (17) by any real-root finder. Simple iterative schemes are found as follows, starting from previous knowledge concerning the general behavior of k/k_o as a function of $\Omega = \omega/\omega_c$.

a. For $\Omega < 1$, one finds that $c \simeq c_b^2$ or $\Omega (c_o/c)^2 \simeq 1$. A good approximation to Eq. (17) is thus

$$(c_o/c)^2 \simeq \Omega^{-1} \left[1 + \frac{\epsilon/\Omega}{\sqrt{\Omega^{-1} - 1}}\right]^{1/2} ; \qquad (18)$$

and a useful iterative calculation to improve on this first guess is

$$(c_o/c)^2_{n+1} = \Omega^{-1} \left[1 + \frac{\epsilon/\Omega}{\sqrt{(c_o/c)^2_n - 1}}\right]^{1/2} , \quad n = 1, 2, 3 \ldots , \qquad (19)$$

where one starts with $(c_o/c)^2_1$ given by Eq. (18).

b. For $\Omega > 1$, one finds $c \approx c_o$, and thus a first approximation to Eq. (17) is

$$(c_o/c)^2 \approx 1 + \frac{(\epsilon/\Omega)^2}{(1-\Omega^2)^2} \; ; \tag{20}$$

and an iterative scheme is given by

$$(c_o/c)^2_{n+1} = 1 + \frac{(\epsilon/\Omega)^2}{\left[1-\Omega^2 (c_o/c)^4_n\right]} \quad n = 1, 2, 3 \ldots \; . \tag{21}$$

where the first guess follows from Eq. (20).

Near $\Omega = 1$ the convergence of these iterative schemes is very slow, and one is advised to use other root-finding schemes; e.g., bisection.

The complex root of Eq. (16) can be found from similar iterative computations. A good first approximation is given by

$$(k/k_o)^2 = (c_o/c)^2 \approx \Omega^{-1} \left[1 - \frac{i\epsilon}{\Omega\sqrt{1-\Omega^{-1}}}\right]^{1/2} \; ; \tag{22}$$

and by iteration one can improve its accuracy according to

$$(c_o/c)^2_{n+1} = \Omega^{-1} \left[1 - \frac{i\epsilon}{\Omega\sqrt{1-(c_o/c)^2_n}}\right] \quad n = 1, 2, 3 \ldots \; . \tag{23}$$

This scheme converges for all values of Ω but is very slow close to the locations of the double real roots discussed in the next section. Between these locations of double real roots this latter iterative scheme converges to a real root that is physically not realistic.

2.4 Results for Fluid-Loaded Thin Plate

The numerical examples in this section refer to a brass plate, with the exception of Fig. 9. The physical parameters for this material are given in Table 1. Figures 3 through 8 are given in non-dimensional form and, therefore, they depend only on the loading parameter ϵ. The thickness of the plate enters only if one wants to infer the dimensional frequency from the value of Ω. Also, in this table derived quantities are given that are important to the analysis; e.g., the loading parameter ϵ and coincidence

frequency w_c. Anticipating the results to be given in a later section for fluid-loaded constrained plates, the parameters for viscoelastic and constraining layers used in those examples are also entered into Table 1.

Figure 3 shows the (real parts of the) roots of Eq. (23), expressing $(k/k_0)^2$ as a function of the dimensionless frequency $\Omega = f/f_c$. The validity of the various roots may be judged by checking whether or not the root satisfies Eq. (17) when it is real, and Eq. (16) when it is complex. Valid roots are designated by solid lines in Fig. 3. Notice that the categories "realistic" and "non-realistic" do not coincide with "real" and "complex." Curve 1 represents a non-radiating root, valid for the whole frequency range, "subsonic," since $c/c_0 = k_0/k < 1$. The value of c/c_0 for this root is shown in Fig. 4, in comparison with its value for an unloaded plate. It is interesting to notice that the phase speed of the flexural waves in the fluid-loaded case does not approach the speed of bending waves in vacuum, rather one has $c/c_b \simeq \epsilon^{-1/5}\Omega^{1/10}$ for $\Omega \to 0$ [5]. For higher frequencies, c/c_0 approaches 1 asymptotically.

The solid part of curve 2 in Fig. 3 represents the real part of $(k/k_0)^2$ for a radiating root. A close-up of curve 2 at lower frequencies is shown in Fig. 5. (Notice the logarithmic scale for the ordinate in Fig. 5.) One sees that there is a gap between the two solid parts of this curve, filled by a pair of real roots that are physically not acceptable. The branch points will be discussed below.

Curve 3 of Fig. 3 shows the real part of a complex root pair that is physically not realistic.

The value of the non-dimensional attenuation α/k' corresponding to the solid part of curve 2, Fig. 3, is shown in Fig. 6. Between the two vertical asymptotes there is no continuation of these complex roots. The situation changes drastically if one introduces even a small loss in the bending stiffness of the plate, by setting $D* = D(1 + i\eta_D)$. Equation (16) now becomes

$$ i\sqrt{1-(k/k_0)^2}\ [1 - \Omega^2 (k/k_0)^4 (1 + i\eta)] + \epsilon/\Omega = 0 \ . \tag{24} $$

Now there is one valid complex root for all frequencies, the attenuation of which is shown in Fig. 7. This is the only valid root left: the valid real root for the lossless case becomes complex and is no longer physically meaningful. The curve in Fig. 7 shows a dip where the relative attenuation approaches the value 0.0025. This value follows from considering Eq. (5) for the case of no fluid loading. Then its right-hand side equals zero, and one has $(k'-i\alpha)^4 D(1+i\eta) - \rho_s h w^2 = 0$. Taking the imaginary part of this equation one finds that to first order in the attenuation α, one has $\alpha/k' \simeq \eta/4$.

It is of interest to study the rule for the location of the two points where the complex roots in Fig. 5 change into a pair of real roots. (Remember that the real part of the root depicted in the figure corresponds to a pair of

complex conjugate roots.) Obviously at these locations there is a double real root, found by setting the derivative of the left-hand side of Eq. (7) with respect to τ equal to 0 [10]. Thus the condition is that

$$5\tau^4 + 6\tau^2 + 1 - \Omega^{-2} = 0 , \qquad (25)$$

with solutions $\tau^2 = -3/5 \pm (4/25 + 1/5 \, \Omega^{-2})^{1/2}$. Both double roots occur for $\Omega < 1$, and thus only the positive root of the solution to Eq. (25) can be used. The given values for τ can be substituted into Eq. (7), and the equation may be numerically solved to give two values for Ω and corresponding values for c/c_o as a function of ϵ. Figures 8a and 8b show the relevant curves, with a few discrete points belonging to familiar materials. Notice that any material with a fluid-loading parameter ϵ greater than the right-hand limit in Fig. 8 will have a continuous complex root for all frequencies, even without damping in the plate. An example is aluminum with $\epsilon = 0.39$ (see Fig. 9). For a thin plate loaded on both sides by the same fluid, the right-hand side of Eq. (2) will be -2p instead of -p. This doubling of the pressure loading has as a consequence that the applicable ϵ in this case is twice that of Eq. (11), and thus several of the materials indicated in Fig. 8 would show this continuous complex root for two-sided fluid loading.

3. FLEXURAL WAVES IN A FLUID-LOADED INFINITE PLATE, EXACT ELASTICITY THEORY

The basic approach to the description according to exact elasticity theory of the propagation of straight-crested waves in a fluid-loaded single plate, and of reflection and transmission by such a plate, is given elsewhere [13]. The main points are repeated here.

The dependence of the field variables on the direction of propagation x and time t for a harmonic wave is given by a factor $\exp[i(\omega t - kx)]$, which is subsequently suppressed. The wave propagation in the plate is described by a potential for irrotational wave motion

$$\phi = A_s \cosh qz + B_a \sinh qz , \qquad (26)$$

and a potential for incompressible waves

$$\psi = C_a \cosh sz + D_s \sinh sz , \qquad (27)$$

where $q^2 = k^2 - k_d^2$ and $s^2 = k^2 - k_s^2$.

Here, k_d is the wavenumber for dilatational waves with propagation speed c_d, and k_s is the wavenumber for shear waves with speed c_s in the plate material. The subscripts a and s in the amplitudes for the potentials (A_s, B_a, C_a, and D_s) refer to antisymmetric and symmetric Lamb waves, which are the generalizations at higher frequencies for flexural and extensional waves, respectively.

One applies the boundary conditions: continuity of normal stress and normal particle velocity and zero shear stress at the faces of the plate. In the case where the same fluid is present at both faces of the plate, one has in addition to the pressure variation at the side of the plate with positive z [given by Eq. (3)], another pressure variation for negative z, given by

$$p_- = p_{o-} \, \text{expi}[\omega t - K_x x + K_z(z+h/2)]. \tag{28}$$

The resulting matrix of the coefficients in the linear equations expressing boundary conditions is shown in Table 2. The origin of the coordinate system is at the center of the plate, and the faces are at $z = \pm\, h/2$.

The various dispersion relations are obtained by equating the determinant value of the appropriate matrix to zero. For fluid on both sides of the plate, this is the full 6×6 matrix of Table 2; for fluid on the positive side, it is the matrix obtained by omitting row 6 and column 6 (for fluid on the negative side one omits row 5 and column 5; but, of course, the result is the same). For a plate in vacuum, rows 5 and 6 and columns 5 and 6 are suppressed.

To appreciate the effects of using exact elasticity theory, the phase speeds of flexural waves and extensional waves are shown in Fig. 10 and are compared with the results of thin-plate theory. The results are given for a 10-cm thick brass plate; the parameters are listed in Table 1.

One sees that the value of the frequency for which the flexural wave speed is equal to the sound speed in the medium, water, is shifted from 3218 Hz for thin-plate theory to 5199 Hz for exact elasticity theory.

The phase speed for a plate loaded on one side is shown in Fig. 11. Notice that in exact elasticity theory there are only two roots in the dispersion equation, depending on the sign of $K_z = \pm \sqrt{k_o^2 - k^2}$. In thin-plate theory there are five roots of the polynomial Eq. (7). The appearance of this figure shows features similar to those encountered in the case of thin-plate theory, see Figs. 4 and 5. There is again a non-radiating root at all frequencies with asymptotic value c_o for $f \rightarrow \infty$; the radiative root consists of two branches, interrupted by a frequency range where there are two real roots that are not physically meaningful. The points where this transition takes place are at frequencies 875 and 3635 Hz. The corresponding curve for α/k' is shown in Fig. 12.

4. HYBRID MODEL OF FLUID-LOADED CONSTRAINED PLATE

4.1 Theory

A model has been developed [3] for constrained layer damping, whereby the base plate is described by exact elasticity theory, while the constraining and damping layers are treated according to the Kerwin model [1].

This hybrid model may be easily extended to include fluid loading by combining the modified boundary condition due to the two extra layers with the fluid loading implicit in the matrix of Table 2.

As derived in Ref. 13, the shear stress τ_{zx} at the side of the plate adjacent to the elastomer layer is not zero, as for an unconstrained plate, but is given by

$$\tau_{zx} = - \frac{1 - (c/c_3)^2}{1 - (c/c_3)^2 + g} \frac{G_2 u}{h_2} , \qquad (29)$$

where c_3 is the thin-plate extensional wave speed of the constraining layer. The elastomer layer has a complex shear modulus G_2 and thickness h_2. The tangential displacement of the surface of the plate is u. The shear parameter g is given by

$$g = G_2 (1 - \nu_3^2)/(k^2 E_3 h_2 h_3) , \qquad (30)$$

where E_3 is Young's modulus, ν_3 Poisson's ratio, and h_3 the thickness of the constraining layer.

The displacement u in Eq. (29) may be expressed in terms of the amplitudes A_s, B_a, C_a, D_s of Eqs. (26) and (27). The result of inserting these into the expression for the shear stress Eq. (29) is a modification of the first four elements of the second row of the matrix in Table 2, assuming that the constraining layer is at the positive z side of the plate. The modified matrix elements m_{2i} are (using the half thickness $d_1 = h_1/2$ of the base plate)

$$m_{21} = 2ikqd_1^2 \cosh(qd_1) + iFkd_1 \sinh(qd_1) ,$$

$$m_{22} = (k^2 + s^2)d_1^2 \cosh(sd_1) + Fsd_1 \sinh(sd_1),$$

$$\qquad (31)$$

$$m_{23} = 2ikqd_1^2 \sinh(qd_1) + iFkd_1 \cosh(qd_1),$$

$$m_{24} = (k^2 + s^2)d_1^2 \sinh(sd_1) + Fsd_1 \cosh(sd_1),$$

where $F = 0.5 (G_2/G_1)(h_1/h_2)[1 - (c/c_3)^2]/[1 - (c/c_3)^2 + g]$. G_1 is the shear modulus of the base plate material.

The dispersion relation for the case where constraining layer and fluid are on the same side is obtained by suppressing row 6 and column 6 in the

matrix. If constraining layer and fluid loading are on opposite sides, column 5 and row 5 are suppressed. If both sides are loaded by fluid, the full 6×6 matrix is used.

4.2 Evaluation of Damping Efficiency in Fluid-Loaded Constrained Plate.

The purpose of constrained-layer damping is to absorb acoustic energy present in a vibrating plate or bar by means of a viscoelastic layer. Therefore, one tries to maximize the energy absorbed by studying the attenuation coefficient for viscous damping α_v as a function of the parameters of the experimental condition. When a constrained layer is loaded by fluid, radiation will take place at certain frequency ranges and it is obviously important to assess what fraction of the total attenuation is due to loss by radiation. Apart from the attenuation by viscous damping, one should therefore also consider the damping efficiency, defined as the fraction of the total absorbed energy that is lost to viscoelastic dissipation.

Let W be the power propagated in the straight-crested wave per unit of width of the plate. Then this damping efficiency may be computed in the case of the hybrid model by evaluating the rate of energy loss by radiation, $(dW/dx)_r$, and the rate of energy loss due to viscoelastic absorption, $(dW/dx)_v$, per unit of distance along the plate.

The energy loss by radiation follows from evaluating the intensity vector $\vec{I}$, expressed in terms of the amplitudes of particle velocity vector $\vec{v}$ and pressure p by $I = \frac{1}{2}\mathrm{Re}(p^*v)$, where Re indicates the real part of a complex quantity, and p^* is the complex conjugate of p. The pressure at the positive side of the plate p_+ is given by

$$p_+ = p_{o+}\exp i\left[\omega t - kx - K_z(z-h/2)\right], \qquad (32)$$

where $k = k' - i\alpha$, and $K_z = K_z' + i K_z''$. The velocity vector $\vec{v}$ is

$$\vec{v}_+ = -\frac{1}{i\rho_o\omega}\vec{\nabla}p_+ = \frac{ip_+}{\rho_o c_o}\left[\frac{k'-i\alpha}{k_o}\ ,\ \frac{K_z'+iK_z''}{k_o}\right]. \qquad (33)$$

The intensity vector is then given by

$$\vec{I} = \frac{|p_{+o}|^2}{2\rho_o c_o}\left[\frac{k'}{k_o}\ ,\ \frac{K_z'}{k_o}\right]; \qquad (34)$$

and its absolute value is given by

$$I = \frac{|P_+|^2}{2\rho_o c_o} \frac{\left[\left(k'\right)^2 + \left(K'_z\right)^2\right]^{1/2}}{k_o} = \frac{|P_+|^2}{2\rho_o c_f} , \qquad (35)$$

where c_f is the phase speed of the radiated wave introduced before. The expression Eq. (35) has the well-known form for plane waves of the free wave speed c_o is replaced by the speed c_f for waves influenced by the presence of the plate. The energy-loss rate per unit of distance due to radiation is thus (suppressing a factor $e^{-2\alpha x}$)

$$\left|\frac{dW_+}{dx}\right|_r = I \cos\delta = \frac{1}{2} \frac{|P|^2}{\rho_o c_f} \cos\delta = \frac{1}{2} \frac{|P_{o+}|^2}{\rho_o c_o} \left(\frac{K'_z}{k_o}\right) . \qquad (36)$$

The computation for the other side gives a similar result,

$$\left|\frac{dW_-}{dx}\right|_r = \frac{1}{2} \frac{|P_{o-}|^2}{\rho_o c_o} \cos\delta . \qquad (37)$$

The rate of energy loss per unit of distance in the x direction in the viscoelastic layer, according to Kerwin's model, is given by

$$\left|\frac{dW}{dx}\right|_v = \frac{1}{2} \frac{\omega G''_2}{h_2} |\xi|^2 , \qquad (38)$$

where ξ is the amplitude of the shear displacement in the elastomer layer, equal to the difference in the displacement of the top and bottom of the layer. This may be written as

$$|\xi|^2 = |\xi/u|^2 \, |u/d_1|^2 , \qquad (39)$$

where

$$\xi/u = - \frac{1 - (c/c_3)^2}{1 - (c/c_3)^2 + g} . \qquad (40)$$

The field quantities p_{o+}, p_{o-}, and (ξ/u) can be obtained from the matrix in Table 1. One can then find the damping efficiency ϵ_D from

13

$$\epsilon_D = \frac{|dW/dx|_v}{|dW/dx|_r + |dW/dx|_v} \cdot \qquad (41)$$

4.3 Comparison of Damping Efficiency in Various Models

The concept of damping efficiency was defined in section 4.2 as the fraction of the total energy loss that is due to damping by the viscoelastic layer. It is quite common to evaluate this efficiency by computing it from the separate cases of a single fluid-loaded plate and a constrained plate in vacuum. This implies the tacit assumption that the radiation by a fluid-loaded constrained plate is the same as the radiation by a simple fluid-loaded plate, and that the viscoelastic damping in a fluid-loaded constrained plate is the same as that in a constrained plate in vacuum. It ignores a possible interaction between the fluid-loading and constraining layers in the composite situation.

In this section, the validity of this assumption is investigated by comparing the damping efficiency for a fluid-loaded constrained plate with a linear combination of the separate cases of a single plate loaded by fluid and a constrained plate in vacuum. The damping efficiency for the first case is computed according to the expression Eq. (41). For the linear combination the attenuation constant for the single fluid-loaded plate α_r is combined with the attenuation constant α_v for the constrained layer in vacuum to give the total attenuation α_T by

$$\alpha_T = \alpha_v + \alpha_r , \qquad (42)$$

and damping efficiency ϵ_D by

$$\epsilon_D = \frac{\alpha_v}{\alpha_v + \alpha_r} \cdot \qquad (43)$$

In the following numerical examples the base plate is 10-cm-thick brass. The elastomer layer is 1.24-mm thick, its shear modulus is chosen to be constant for the whole frequency range. Of course, this is physically unrealistic since the property of viscoelasticity is by nature dependent on frequency. The constancy of G, though, brings out the geometry and frequency dependence of the damping, separated from viscoelastic behavior as a function of frequency. A value of $G_2 = 10(1+i)$ MPa was chosen. The constraining layer is 2.48-mm thick. Table 1 shows the parameters of the constrained plate and of the acoustic medium.

Figure 13 shows the comparison for a constrained plate loaded by a fluid at the side of the constraining layer with the separate cases of a single plate with a fluid layer and a constrained layer in vacuum. One sees clearly the two ranges of high damping due to radiation and, in between these, the hump due to viscoelastic damping. It appears, at least at the scale of the graph, that the total attenuation is practically due to one or the other effect with only some visible discrepancy at the higher end of the viscoelastic hump.

The comparison of the damping efficiency computed for the two cases (the first being the linear combination of a single plate in the fluid with a constrained plate in vacuum, the second being a fluid-loaded constrained plate) is shown in Fig. 14. Again, for a rather large frequency range the differences are small. At the lower frequency end there is a discrepancy that apparently corresponds to the fact that the absorption in the viscoelastic layer is influenced by the presence of the fluid. At the high-frequency side one sees that the efficiency computed from the linear combination turns up sharply at about 40 kHz. This is due to an effect already discovered [13]. For high frequencies the loading of one face of the plate by a fluid forces the action (i.e., the displacement of the plate particles) to the unloaded side so that the radiation drastically diminishes. This suggests that in this frequency range it is better to damp a wave by applying the constraining layers at the side of the plate opposite to the loading fluid. The effect of this can be seen in the total attenuation (Fig. 15) where attenuation due to radiation falls off for both cases (fluid on the same side or opposite side to the constraining layers) while the viscoelastic damping remains intact for the latter case. The effect on damping efficiency is clearly visible in Fig. 16.

When the attenuation for one-sided loading is compared with the case of fluid-loading on both sides (Fig. 17), one sees that indeed the radiation stays high for the symmetric situation. Accordingly, the damping efficiency (Fig. 18) shows a steady decrease with f and is well approximated by a linear combination of separate radiation and viscoelastic damping (dashed curve). Notice that in Figs. 16 through 18 only the high-frequency part of the curves is shown. The scale of the abscissa is kept the same to facilitate comparison with Figs. 12 through 14.

5. CONCLUSIONS

This study shows that for a sizable frequency-range, it is a good approximation to obtain the damping and radiation in a fluid-loaded composite plate by a linear combination of the attenuation in a single plate in a fluid and a composite plate in vacuum.

At both the high- and low-frequency ends of this range, though, discrepancies occur between the linear combination of the two cases of a single plate in a fluid and a constrained plate in vacuum and the computation based on a fluid-loaded constrained plate by the hybrid model. This necessitates, in general, the study of the complete fluid-loaded composite situation, in order to predict the total attenuation, and especially the damping efficiency.

REFERENCES

1. E.M. Kerwin, "Damping of flexural waves by a constrained viscoelastic layer," *J. Acoust. Soc. Am.* **31**, 952-962 (1959).

2. P.J. Torvik, "The Analysis and design of constrained layer damping treatments," in *Damping Applications for Vibrational Control*, P.J. Torvik, ed. (The American Society of Mechanical Engineers, New York, 1980), pp. 85-112.

3. Pieter S. Dubbelday, "Constrained-layer model investigation based on exact elasticity theory," *J. Acoust. Soc. Am.* **80**(4), 1097-1102 (1986).

4. P.M. Morse and K.U. Ingard, *Theoretical Acoustics* (McGraw-Hill, New York, 1968), Sec. 10.1.

5. M.C. Junger and D. Feit, *Sound, structures, and their interaction*, 2nd ed, (MIT Press, Cambridge, 1972, 1986), Ch. 8.

6. David Feit, "Pressure Radiated by a Point-Excited Elastic Plate," *J. Acoust. Soc. Am.* **40**, 1489-1494 (1966).

7. P. Ranganath Nayak, "Line Admittance of Infinite Isotropic Fluid-Loaded Plates," *J. Acoust. Soc. Am.* **47**, 191-201 (1970).

8. Alan D. Stuart, "Acoustic radiation from submerged plates. I. Influence of leaky wave poles," *J. Acoust. Soc. Am.* **59**(5), 1160-1169, (1976).

9. Alan D. Stuart, "Acoustic radiation from submerged plates. II. Radiated power and damping*," *J. Acoust. Soc. Am.* **59**(5), 1170-1174, (1976).

10. Mauro Pierucci and Thomas S. Graham, "A study of bending waves in fluid-loaded thick plates," *J. Acoust. Soc. Am.* **65**(5), 1190-1197, (1979).

11. Mauro Pierucci, "Additional solutions to the free bending waves of a fluid-loaded thick plate," *J. Acoust. Soc. Am.* **70**(3), 866-869 (1981).

12. Ref. 10, p. 1196.

13. P.S. Dubbelday, "Application of a new-complex root-finding technique to the dispersion relations for elastic waves in a fluid-loaded plate," *SIAM J. Appl. Math.* **43**, 1127-1139 (1983).

Table 1. Material Parameters and Derived Quantities

1. **Base plate, brass**

thickness	$h_1 = 10$ cm	shear modulus	$G_1 = 38.0$ GPa
Young's modulus	$E_1 = 104$ GPa	extensional wave speed (thin-plate)	$c_p = 3765$ m/s
Poisson's ratio	$\nu_1 = 0.37$		
density	$\rho_s = 8500$ kg/m^3		

shear wave speed $c_s = 2113$ m/s
bending stiffness $D^s = 10.0$ MN m
fluid-loading parameter $\epsilon = 0.086$
coincidence frequency $f_c = 3212$ Hz
   (thin-plate)

2. **Viscoelastic layer (hypothetical)**

thickness	$h_2 = 1.24$ mm
shear modulus	$G_2 = 10$ MPa
loss tangent in shear modulus	$\beta = 1.0$

3. **Constraining layer, aluminum**

thickness	$h_3 = 2.48$ mm
Young's modulus	$E_3 = 71$ GPa
Poisson's ratio	$\nu_3 = 0.33$
density	$\rho_3 = 2700$ kg/m^3

4. **Fluid, fresh water**

density	$\rho_o = 998$ kg/m^3
wave speed	$c_o = 1481$ m/s

Table 2 – Matrix of Coefficients of Equations Describing Wave Propagation in Fluid-Loaded Single Plate. Exact elasticity theory. Here d is the half thickness of the plate $d = h/2$.

Field variables---->

B_s/d^2	C_s/d^2	A_s/d^2	D_s/d	$p_{o+}/(\rho_o c_s^2)$	$p_{o-}/(\rho_o c_s^2)$
$(k^2+s^2)d^2 \sinh(qd)$	$-2iksd^2 \sinh(sd)$	$(k^2+s^2)d^2 \cosh(qd)$	$-2iksd \cosh(sd)$	ρ_o/ρ_s	0
$2ikqd^2 \cos(qd)$	$(k^2+s^2)d^2 \cosh(sd)$	$2ikqd^2 \sinh(qd)$	$(k^2+s^2)d^2 \sinh(sd)$	0	0
$-(k^2+s^2)d^2 \sinh(qd)$	$2iksd^2 \sinh(sd)$	$(k^2+s^2)d^2 \cosh(qd)$	$-2iksd \cosh(sd)$	0	ρ_o/ρ_s
$-2ikqd^2 \cosh(qd)$	$-(k^2+s^2)d^2 \cosh(sd)$	$2ikqd^2 \sinh(qd)$	$(k^2+s^2)d^2 \sinh(sd)$	0	0
$qd \cosh(qd)$	$-ikd \cosh(sd)$	$qd \sinh(qd)$	$-ikd \sinh(sd)$	$\dfrac{iK_s d}{(k_s d)^2}$	0
$qd \cosh(qd)$	$-ikd \cosh(sd)$	$-qd \sinh(qd)$	$ikd \sinh(sd)$	0	$\dfrac{-iK_s d}{(k_s d)^2}$

18
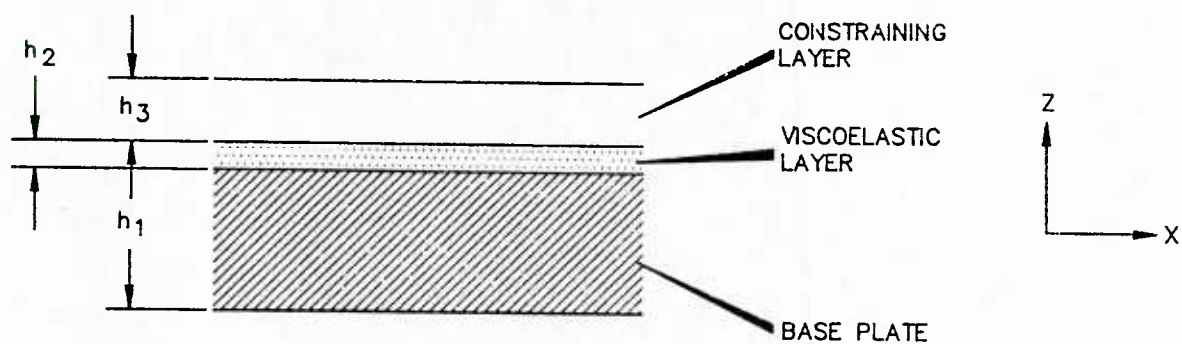
Fig. 1 - Geometry of constrained layer.
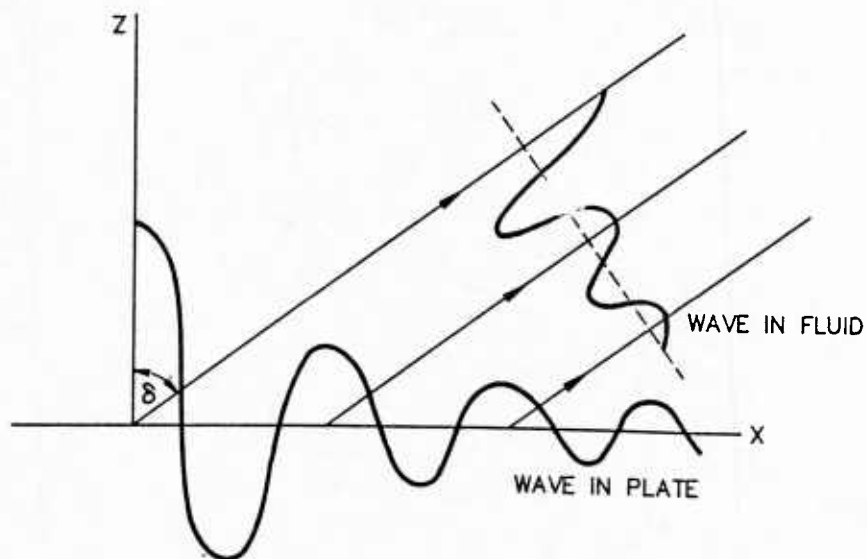
Fig. 2 - Relation between wave-amplitude variation in the plate and in the fluid.
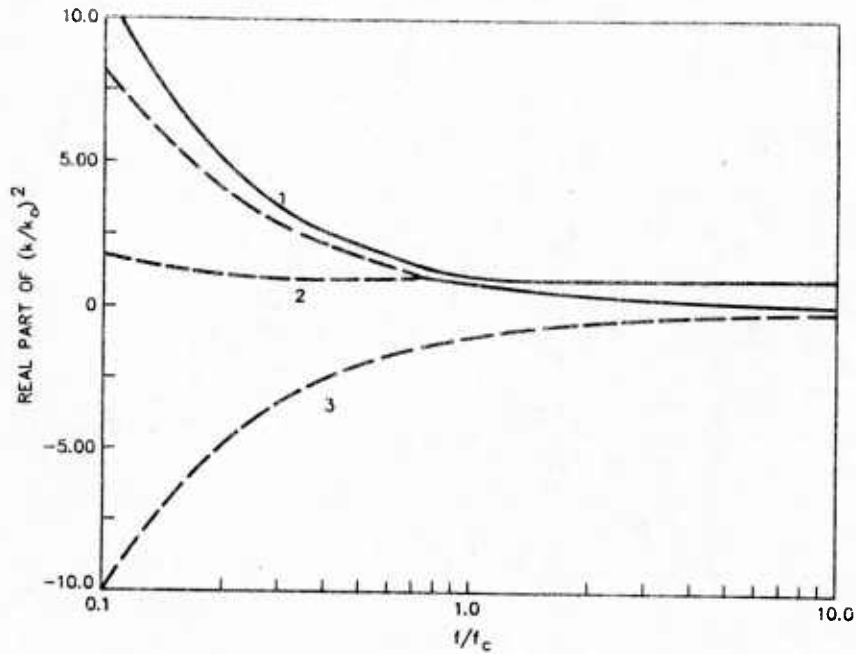
Fig. 3 - Real part of the roots $\eta = (k/k_o)^2$ of Eq. 22 for flexural waves in fluid-loaded plate. The solid (parts of) curves are physically realistic.

  Curve 1 Real subsonic root

  Curve 2 ——————— radiating root

      - - - - - - - two real roots

      The branch point is located at $f/f_c = 0.725$, $(k/k_o)^2 = 1.136$

  Curve 3 - - - - - - - complex root
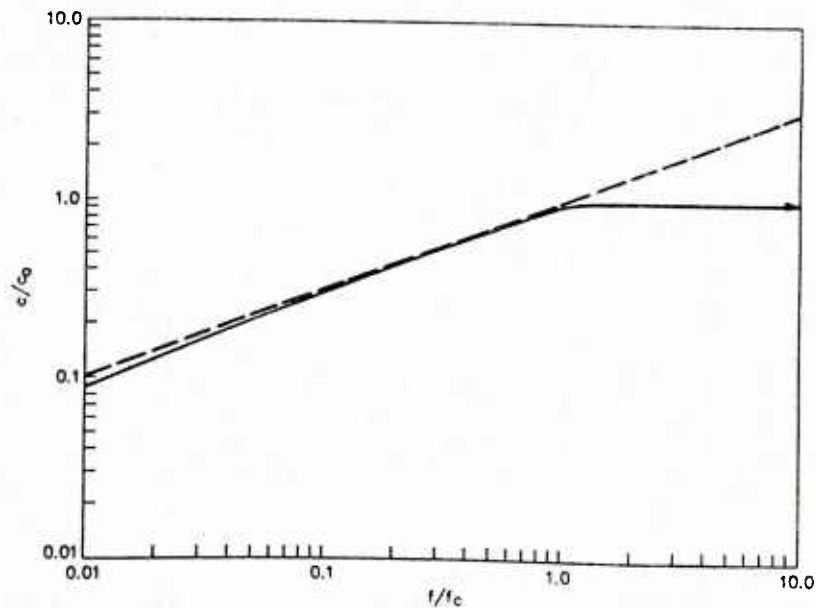
Fig. 4 - Relative wave speed of non-dissipative subsonic flexural wave in thin plate as a function of relative frequency. ——————— Loaded by fluid on one side. - - - - - - - in vacuum.
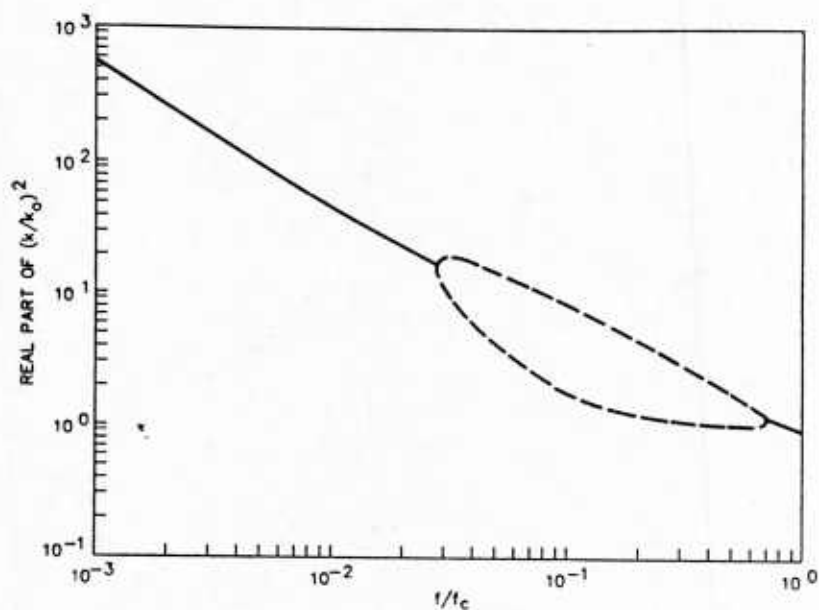
Fig. 5 - Fluid-loaded thin plate. ——————— Acceptable complex root. -------- Non-realistic real roots. Extension of curve 2, Fig. 3 for low frequency. The branch points are located at f/f_c = 0.725; $(k/k_o)^2$ = 1.136 and f/f_c = 0.0276; $(k/k_o)^2$ = 16.59.
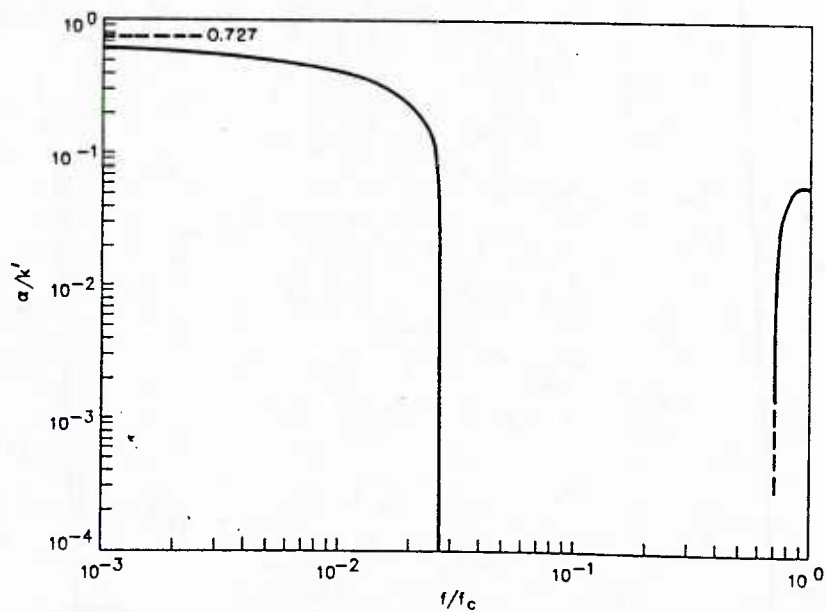
Fig. 6 - Fluid-loaded thin plate. Non-dimensional attenuation α/k' for radiating root of Fig. 5
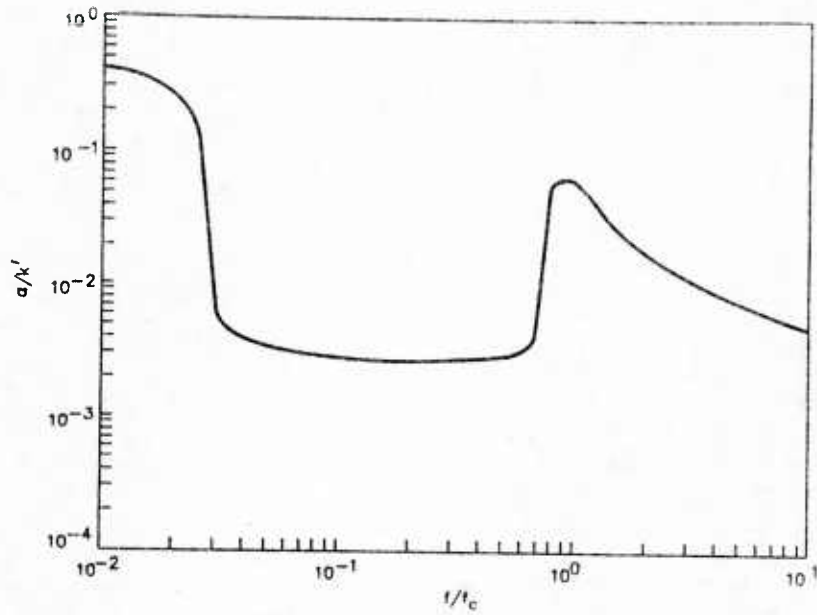
Fig. 7 - Fluid-loaded thin plate. Non-dimensional attenuation, α/k' for plate with loss tangent $\eta = 0.01$ in bending stiffness D.
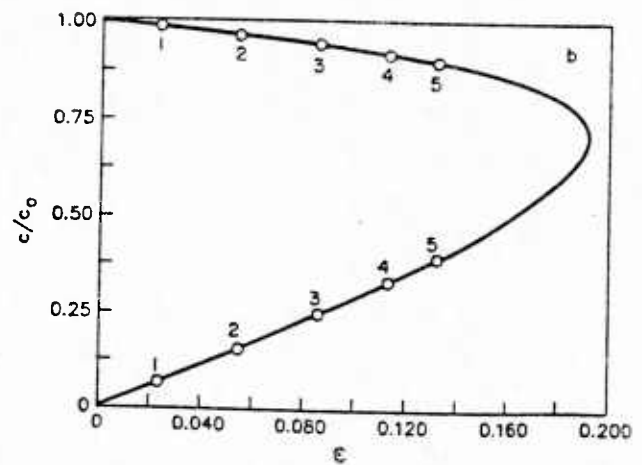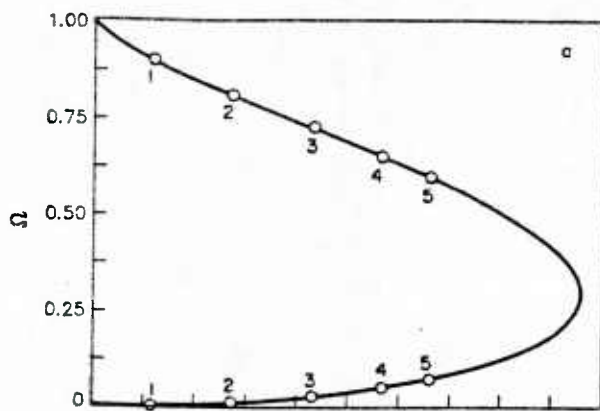
Fig. 8 - Thin plate loaded on one side by water. Values of double real roots, as a function of fluid-loading parameter ϵ.

Discrete points:
- 1 - lead
- 2 - silver
- 3 - brass
- 4 - nickel
- 5 - steel

a) $\Omega = \omega/\omega_c$

b) c/c_o

22
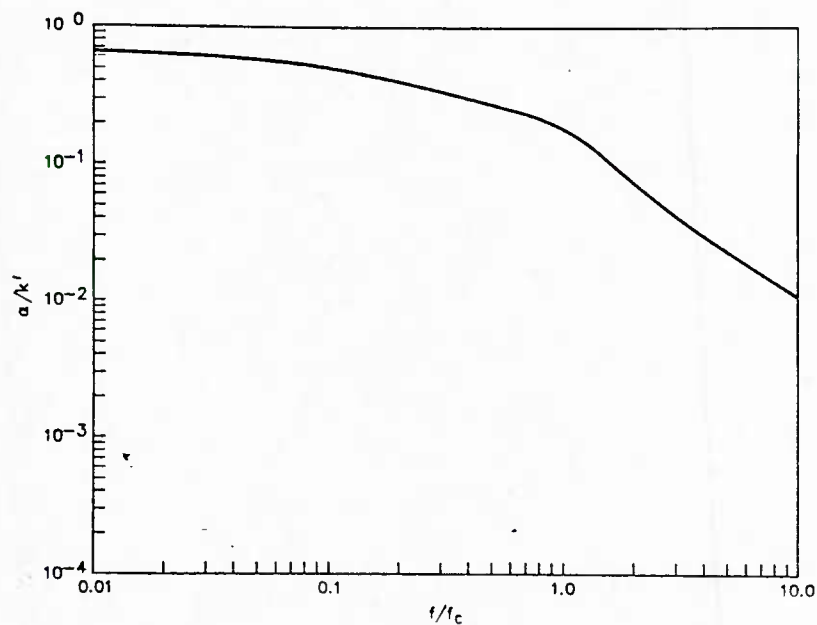
Fig. 9 – Thin aluminum plate loaded on one side by water. Non-dimensional attenuation a/k' as a function of relative frequency f/f_c.
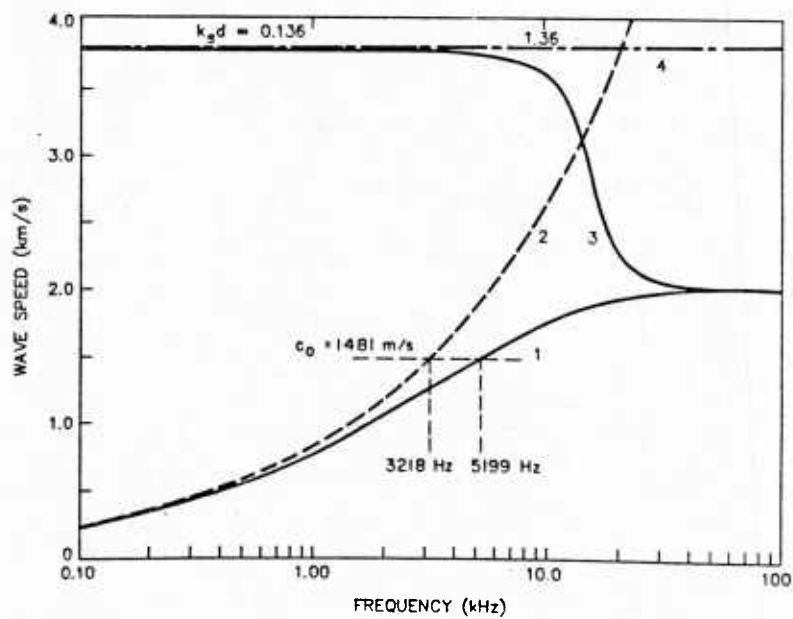
Fig. 10 – Phase speed of waves in infinite brass plate of 10 cm thickness in vacuum.
Antisymmetric (flexural) wave
1. Exact theory
2. Thin-plate theory
Symmetric (extensional) wave
3. Exact theory
4. Thin-plate theory
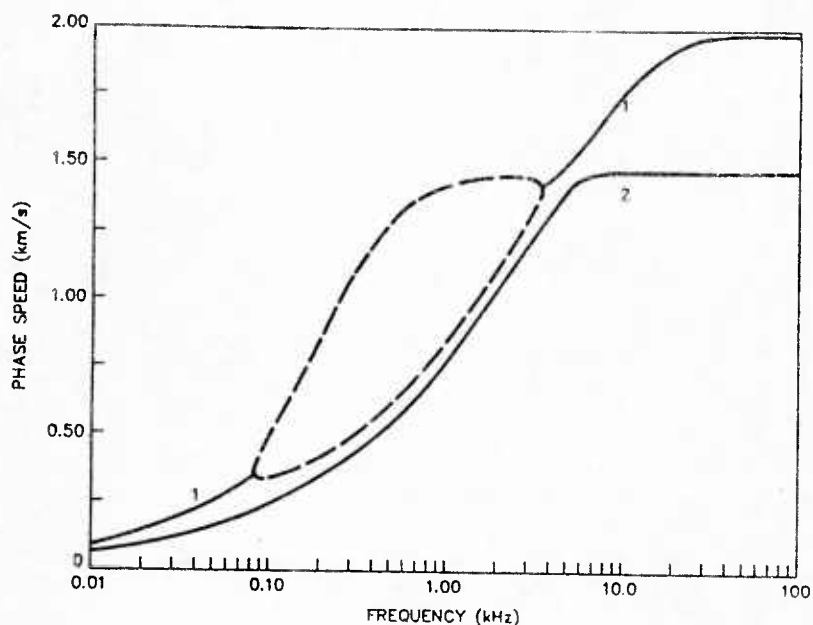
Fig. 11 – Phase speed of 10-cm thick brass plate, loaded by water on one side. The solid curves represent physically acceptable roots.
1. (solid parts) radiative root
2. Non-dissipative root
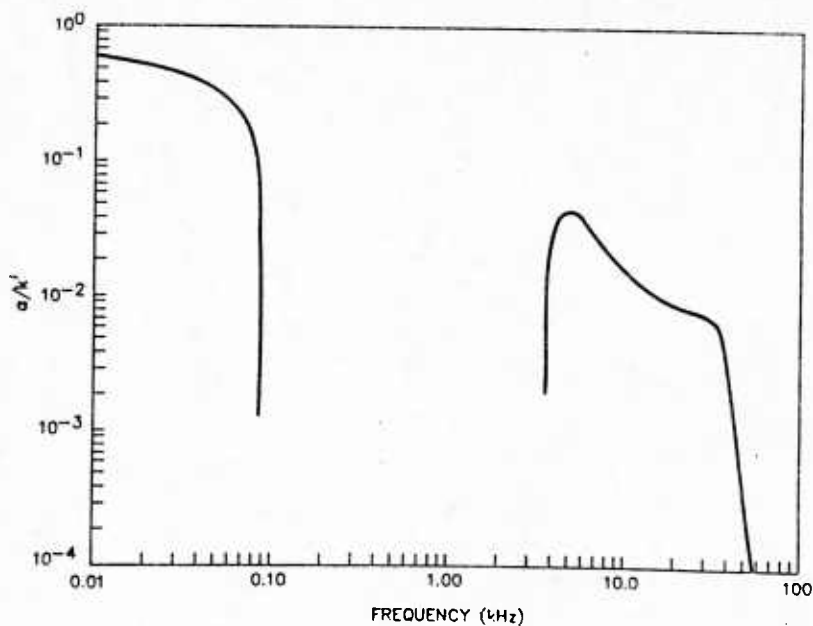
Fig. 12 – Non-dimensional attenuation α/k' of radiating waves in 10-cm thick brass plate loaded on one side by water.
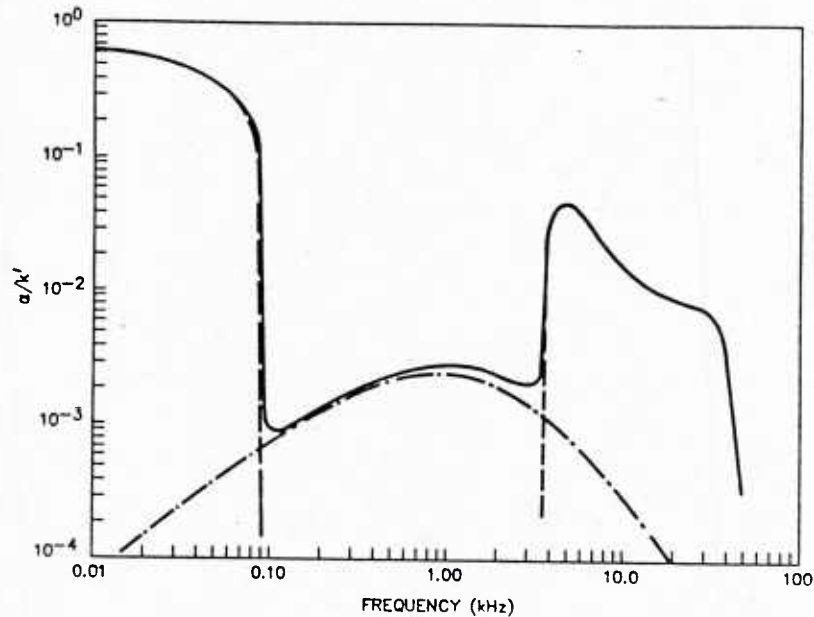
Fig. 13 - Comparison of attenuation coefficients. ——————— Total dimensionless attenuation α/k' of constrained plate, loaded by water on the side of the damping layers. -------- Attenuation of single plate loaded by water on one side. -·-·-·-· Damping of constrained plate in vacuum.
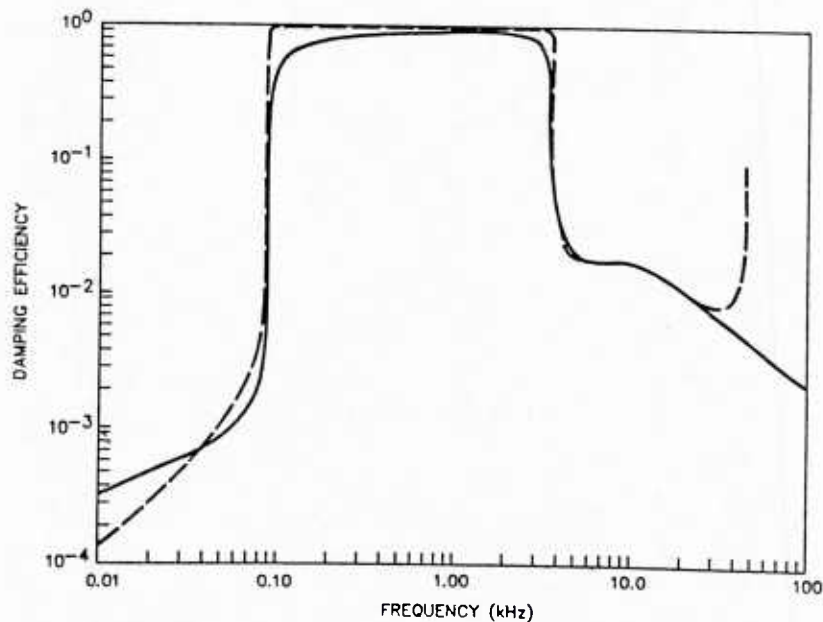
Fig. 14 - Comparison of damping efficiency. ——————— Constrained brass plate loaded by water on side of damping layers. -------- Computed by linear combination of radiation damping of single plate loaded on one side, and viscoelastic damping of constrained plate in vacuum.
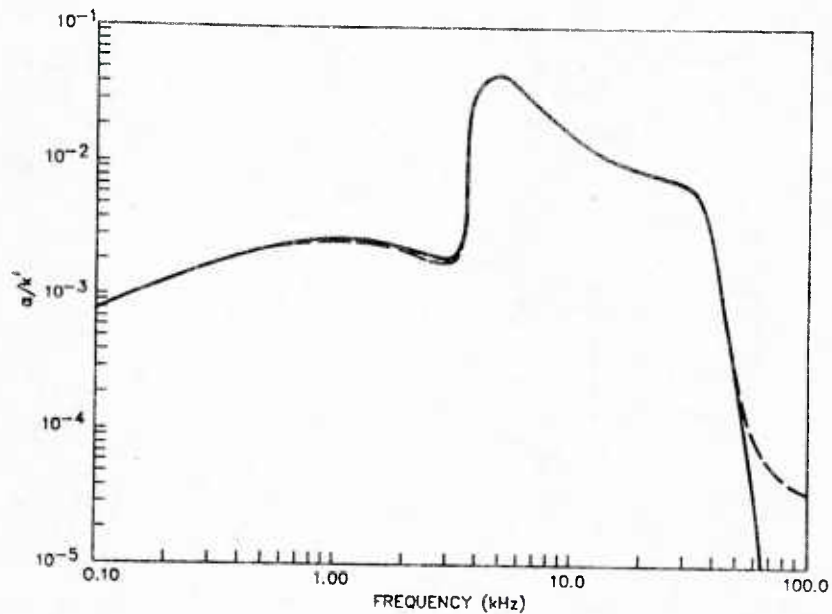
Fig. 15 - Comparison of total attenuation. ───────── Constrained brass plate loaded by water on side of damping layers. ───────── Constrained brass plate loaded by water on opposite side from damping layers.
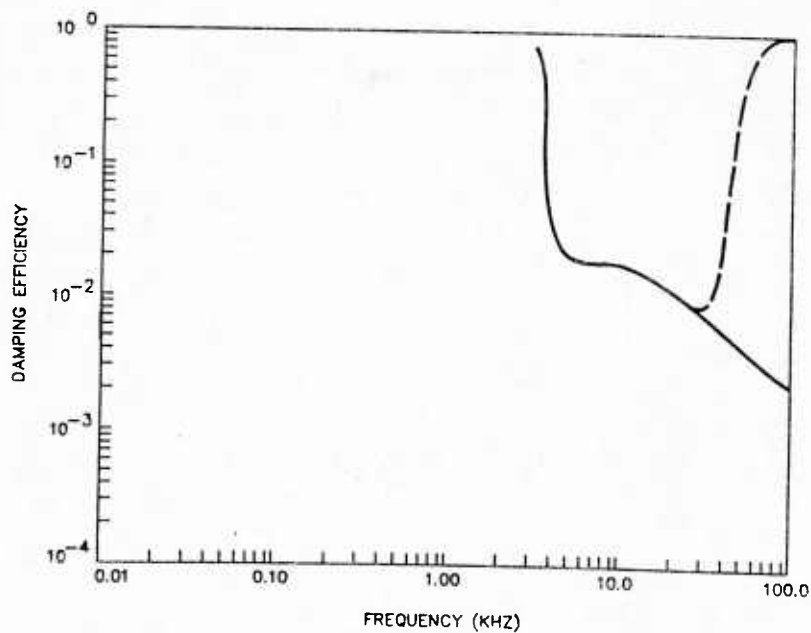

Fig. 16 - Comparison of damping efficiency. ───────── Constrained layer loaded by water on side of damping layer. ───────── Constrained layer loaded by water on opposite side from damping layers.
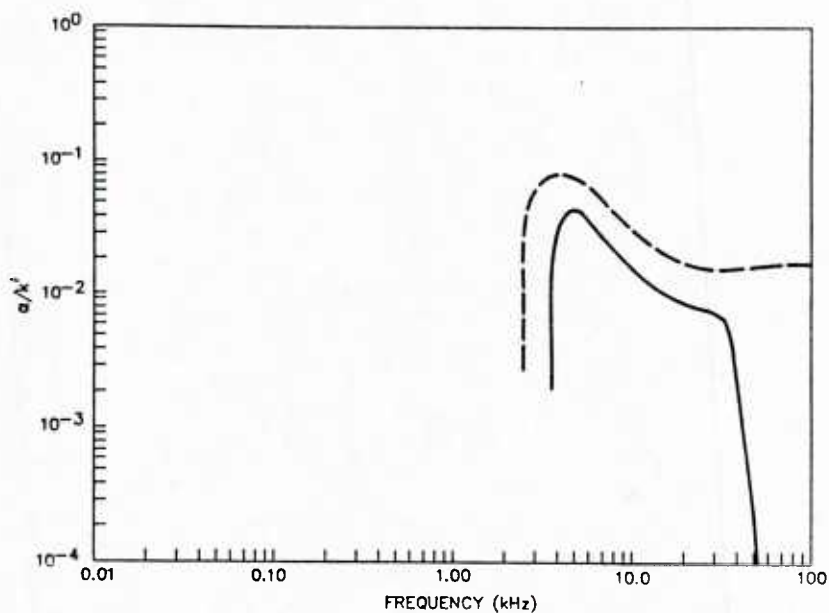
Fig. 17 – Comparison of total attenuation. ——————— Constrained brass plate loaded by water on side of damping layers. -------- Constrained brass plate loaded by water on both sides.
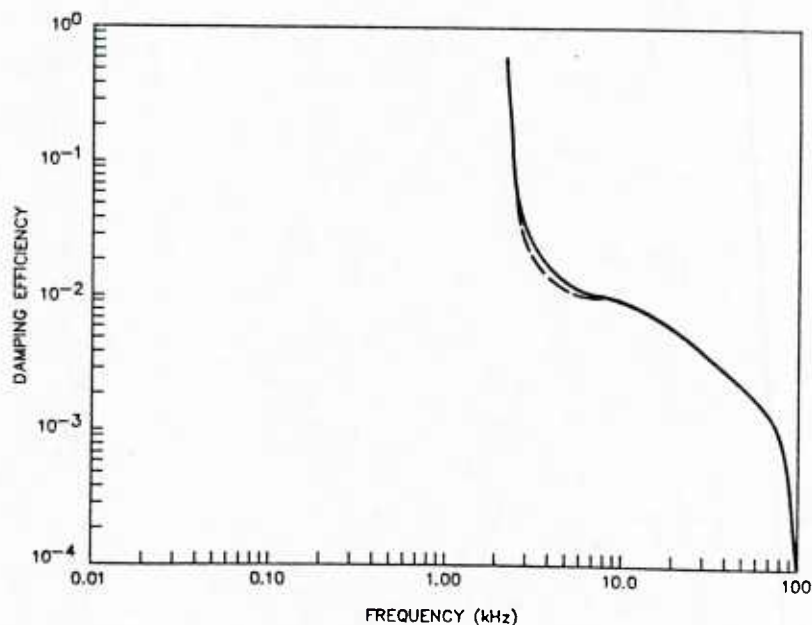

Fig. 18 – Comparison of damping efficiency. ——————— Constrained layer loaded by water on both sides. -------- Computed by linear combination of attenuation of radiation damping for single plate, loaded on both sides, and viscoelastic damping of constrained plate in vacuum.

U230623

Superintendent
Naval Postgraduate School
Attn: Technical Library
Monterey, CA 93943